Electronic Supporting Information

pH-responsive swimming behavior of the light-powered rod-shaped micromotors

Srikanta Debata[a], Suvendu Kumar Panda[a], Satyaprakash Trivedi[a], William Uspal[b*], and Dhruv Pratap Singh[a*]

[a]*Department of Physics, IIT Bhilai, Kutelabhata, Durg, Chattisgarh, 491001, India.*

[b]*Department of Mechanical Engineering, University of Hawai'i at Mānoa, 2540 Dole Street, Holmes Hall 302, Honolulu, HI 96822, USA.*

[*]Corresponding Author: *uspal@hawaii.edu, dhruv@iitbhilai.ac.in*

1. Guide to supplementary Videos:

Video S1: Video shows the head-forward motion of micromotors at pH 4 of the peroxide medium (5% v/v) under low-intensity UV light irradiation. The video plays at 1X speed.

Video S2: Video shows the tail-forward motion of micromotors at pH 8 of the peroxide medium (5% v/v) under low-intensity UV light illumination. The video plays at 1X speed.

Video S3: Video shows the rotational motion of micromotors at pH 9 of the peroxide medium (5% v/v) under low-intensity UV light illumination. The video plays at 1X speed.

2. Supplementary figure description and discussion

2.1 UV-vis absorption analysis:

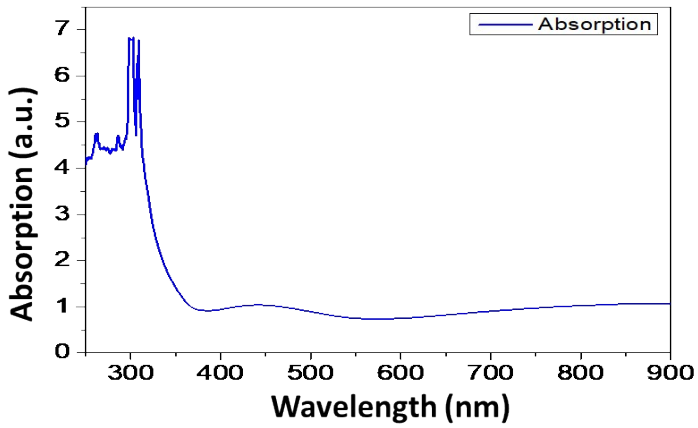

Fig. S1 Absorption spectra show the absorbance in the lower wavelength UV region.

2.2 Strongly tilted state:

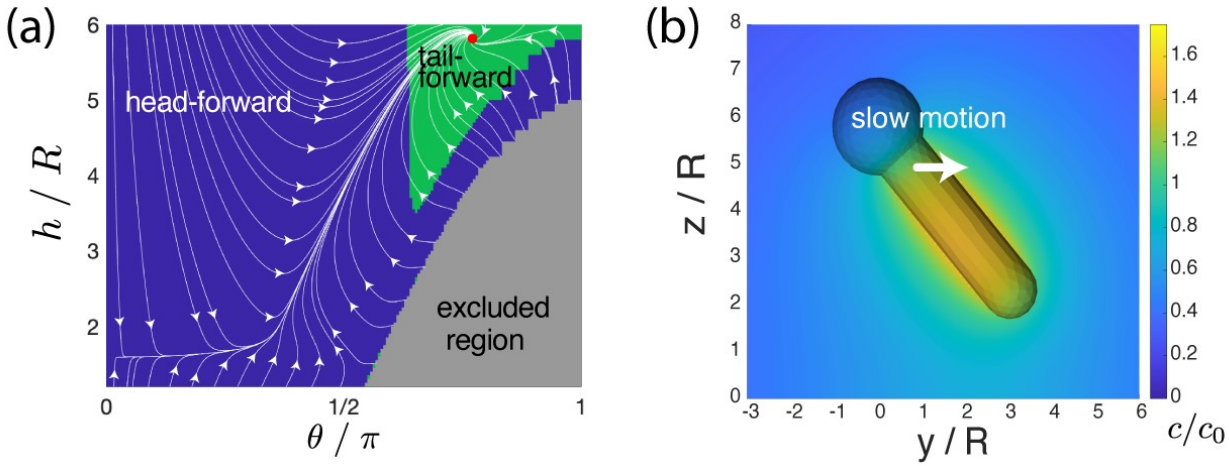

Fig. S2. Strongly tilted state. (a) Phase portrait for b_c = -0.5, b_i = -0.2, and $U_0 =$ 190 $\mu m/s.$ (b) Particle configuration and concentration field for the same parameters as in (a). The particle has a strong tilt towards the wall. The particle has a slow "sliding" speed $|U_y| =$ 0.53 $\mu m/s$.

2.3 Discussion on MSD data:

To understand the quantitative aspect of motion, let's take the standard expression of the mean square displacement (MSD) equation for a 2-dimensional case, which has both Brownian motion term and active motion term.

The equation can be written as,

$$MSD = 4D\Delta t + \frac{v^2 {\tau_R}^2}{2}\left[\frac{2\Delta t}{\tau_R} + e^{-2\Delta t/\tau_R} - 1\right] \quad (1)$$

Where D is the diffusion coefficient, t is the time,

v is the velocity, and τ_R is the inverse rotational diffusion coefficient.

The inverse rotational diffusion coefficient for our system can be calculated as,

$$\tau_R = \frac{1}{D_R}$$

Further,

$$\tau_R = \frac{8\pi\eta R^3}{K_B T}$$

On solving the equation, we are getting a value of τ_R as around 22 sec for our particle.

For Brownian motion, the MSD from equation (1) can be written as,

$$MSD = 4D\Delta t$$

For the passive state, the MSD is directly proportional to Δt. From Fig. S3, when the light is turned off the micromotors are exhibiting random Brownian motion and we are getting a straight-line behavior of the plot.

Over some period when $\Delta t \ll \tau_R$, the MSD of equation (1) will change to,

$$MSD = 4D\Delta t + v^2\Delta t^2$$

The equation shows the MSD during propulsion of a particle at the time interval of $\Delta t \ll \tau_R$. From the expression, MSD is proportional to the square of the time interval and the nature of the plot will be parabolic. In our case also, the time interval Δt is less than that of calculated τ_R and in that interval the nature of the curve (see Fig. S3) is parabolic which satisfies the mathematical equation. The red curve in Fig. S3 shows the behavior of micromotors when the light is turned on.

The persistence length is the distance over which particle's motion remains correlated. The concept of persistence length helps to describe how long a particle's trajectory tends to align with its previous direction before randomness takes over. The persistent length in one direction can be calculated as,

Persistence length, $L = speed\ of\ the\ particle\ \times\ \tau_R$

By calculating from the MSD plot, the persistence length of micromotors during active swimming is found to be around 44 microns. This value is the result of theoretical calculations and experimental results are also matching with it.

Finally, when the $\Delta t \gg \tau_R$, a transition to diffusive regime happened with an enhanced coefficient of diffusion. At the same time scale the equation (1) changes to

$$MSD = \left(4D + v^2\tau_R\right)\Delta t$$

The equation shows a proportionality relation of MSD with time interval and the nature of curve will be a straight line. To observe a transition to diffusive regime the condition is $\Delta t \gg \tau_R$, which is not considered in the plot in this study and therefore the condition is not satisfied. This is the reason we are not observing a transition to the diffusive regime in the given MSD plots.

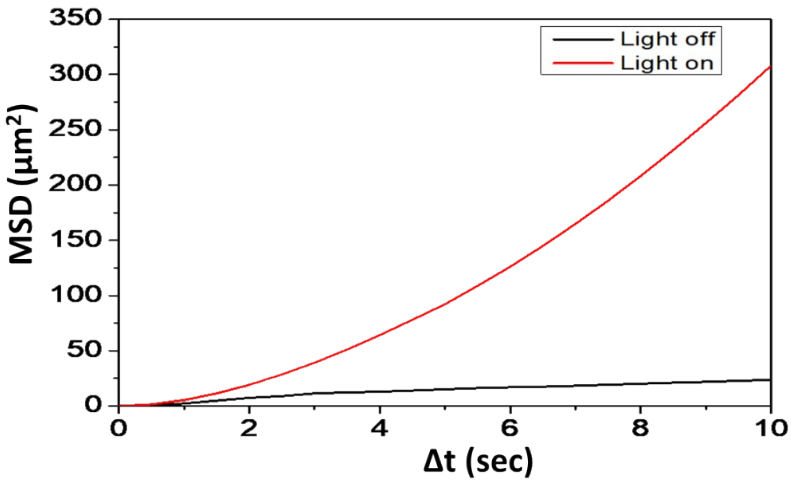

Fig. S3 MSD vs. time interval plot for the micromotors during light on (red color) and off (black color) conditions in pH 4 peroxide solution (2.5% v/v). Light on and off condition corresponds to the motile (active) and non-motile (Brownian) state of the micromotors respectively.

2.4 Observation of tilting state:

The tilting of the micromotor during the rotational motion at a high pH as shown in Fig. 4c, has been suggested by the theoretical analysis. The measurement or a clear confirmation of the tilt angle in experiments is very difficult. Considering the optical arrangement that allows the visualization in the X-Y plane, it is not possible to have a clear visualization of micromotors in the Z plane which limits the information about the tilt. However, it can be noted that because of a tight focus in X-Y plane, any movement/tilt in the Z plane will make the micromotor go out of focus and show a distorted or blurred image. We can see this in the images in Fig. S4. In the images, we see that the micromotor is very clear as well as appears a little bit longer during translation compared to that of the rotational motion. This is an indirect indication of the tilt of the micromotors during rotation at high pH.

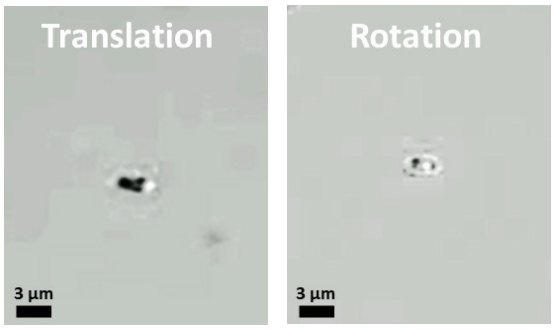

Fig. S4 The snapshot of a single micromotor during translational and rotational motion.

3. Mathematical formulation of the model

We focus on qualitatively capturing the transition between two states: from fast, "head-forward" motion, with the rod axis parallel to the substrate, to tilted, "tail-forward" motion. To this end, we use a simple model, common in the active colloids literature, that resolves the chemical activity of the particle and hydrodynamic flow of the solution. The geometry of the particle is shown in Fig. 5 in the main text. The axis of symmetry of the particle is aligned with the z-direction, and the center of the sphere is located at the origin. The radius of the spherical "head" R provides a length scale for specifying the particle

geometry. The spherical head meets the cylindrical "tail" at $z/R = 0.8.$ The radius of the cylinder is $R_c = 0.6R.$ The cylinder is capped by a hemisphere, with its base located at $(0,0,4.4R)$. The cylindrical region of the particle, as well as its small hemispherical cap, will be regarded as chemically active TiO_2, and the rest of the particle (the open sphere) will be considered chemically inert silica. We will consider this particle in free space (unbounded solution) and confined by a hard planar wall located at z = 0. When we consider a particle near a planar wall, the center of the sphere (no longer located at the origin) will define the particle position $\vec{x}_p = (0,0,h)$, where h is the height of the particle of the wall. The angle of the sphere-to-hemisphere axis with respect to the wall normal is θ. For example, $\theta = 0$ for a particle with its axis aligned with the wall normal, and with its spherical head close to the wall. Likewise, $\theta = 90^{\circ}$ for a particle with its axis parallel to the wall.

Now we turn to the chemical activity of the particle. While it is possible to implement the redox reaction scheme in Eq. 1 (main text) in the framework of our model, it would introduce additional modeling considerations, e.g., which regions of the "tail" to designate as cathode, and which as anode. Instead, we choose to coarse-grain the details of the reaction scheme in Eq. 1, and we approximate that the entire "tail" of the particle as the source of a chemical "product," emitted at a steady and spatially uniform rate. The distribution of the reaction product in the solution is governed by Laplace's equation, $\nabla^2 c = 0$, where $c(\vec{x})$ is the concentration (number density) of the reaction product at a location $\vec{x}$ in the solution. The concentration is subject to the boundary conditions $-D\nabla c \cdot \hat{n} = \kappa$ on the tail, $\nabla c \cdot \hat{n} = 0$ on the spherical "head," and $c(\vec{x}) \to 0$ as $|\vec{x}| \to \infty$. Additionally, for a particle near a planar wall, $\nabla c \cdot \hat{n} = 0$ on the wall. Here, D is the diffusion coefficient of the product molecule, the surface normal $\hat{n}$ is defined to point into the liquid solution, and κ is the rate of production (per unit time, per unit area) of the product molecule. To solve Laplace's equation, we mesh

the surface of the particle and use the boundary element method. When we wish to account for the planar wall, we use the appropriate Green's function. The concentration is obtained in terms of a characteristic concentration $c_0 = |\kappa R/D|$.

Next, we consider the hydrodynamic flow. This flow is governed by the Stokes equation, $-\nabla p + \mu\nabla^2\vec{u} = 0$, where $p(\vec{x})$ is the pressure in the fluid, $\vec{u}(\vec{x})$ is the fluid velocity, and μ is the dynamic viscosity of the solution, and the incompressibility condition, $\nabla \cdot \vec{u} = 0$. The flow is subject to the boundary conditions $\vec{u} = \vec{U} + \vec{\Omega} \times (\vec{x} - \vec{x}_p) + \vec{u}_s(\vec{x})$ on the surface of the particle and $\vec{u}(\vec{x}) \to 0$ as $|\vec{x}| \to \infty$. Additionally, for a particle near a planar wall, $\vec{u} = 0$ on the wall. Here, $\vec{U}$ and $\vec{\Omega}$ are the (unknown) translational and angular velocities, respectively, of the particle. The quantity $\vec{u}_s(\vec{x})$, the so-called slip velocity, provides the interfacial actuation that drives particle motion. It is obtained from solution of the previous problem by $\vec{u}_s(\vec{x}) = -b(\vec{x})\nabla_{||}c$. Here, the quantity $b(\vec{x})$, the so-called surface mobility, encapsulates the effective, molecular scale interaction between the particle surface and the product molecule. We assume that it takes piecewise constant values: $b = b_i\, b_0$ on the inert spherical head, and $b = b_c\, b_0$ on the catalytic tail, where b_0 is a characteristic value of the surface mobility that carries the dimensions. (The quantities b_i and b_o are dimensionless.) The surface gradient operator is defined by $(\vec{I} - \hat{n}\hat{n}) \cdot \nabla$. The equations are closed by writing a force balance condition, $\vec{F}_H + \vec{F}_e = 0$, and torque balance condition, $\vec{\tau}_H + \vec{\tau}_e = 0$. Here, $\vec{F}_H = \int \vec{\vec{\sigma}} \cdot \hat{n}\, dS$ is the hydrodynamic force on the particle, where the integral is taken over the particle surface and $\vec{\vec{\sigma}} = -p\vec{\vec{I}} + \mu(\nabla\vec{u} + \nabla\vec{u}^T)$ is the Newton stress tensor. The quantity $\vec{F}_e$ represents any external forces on the particle. Likewise, $\vec{\tau}_H = \int (\vec{x} - \vec{x}_p) \times \vec{\vec{\sigma}} \cdot \hat{n}\, dS$ is the hydrodynamic torque on the particle, and $\vec{\tau}_e$ represents any external torques exerted on the

particle. The equations can be solved numerically for $\vec{U}$ and $\vec{\Omega}$ by using the Lorentz reciprocal theorem and the boundary element method, as detailed in previous work. The velocity is obtained in terms of a characteristic velocity $U_0 = |b_0\kappa/D|$. For a particle in free space with $\vec{F}_e = 0$ and $\vec{\tau}_e = 0$, we numerically obtain the free space velocity as a function of the surface chemistry parameters, $U_{fs}/U_0 = 0.0943b_i - 0.0298\, b_c$. This relation allows us to connect our numerical calculations with experimental observations. If a characteristic experimental velocity of the particle, in meters per second, is v_f, then the relation $U_0 = |v_f/U_{fs}|$ gives U_0 with units of meters per second.

For a particle near a wall, we include external forces and external torque. Specifically, we account for gravitational effects (buoyant weight and gravitational torque), and also include a short-ranged repulsive force and torque from the wall. The buoyant weight $\vec{F}_g$ is approximated as the buoyant weight of a silica sphere of radius $R = 0.5\,\mu m$ and density $\rho_{SiO2} = 2196\ kg/m^3$ in water ($\rho_{H2O} = 1000\ kg/m^3$), plus the buoyant weight of a cylindrical rod with radius $R_c = 0.8R$ and density $\rho_{TiO2} = 4000\ kg/m^3$. For the gravitational torque with respect to the sphere center $\vec{\tau}_g$, we use the weight of the rod and the lever arm $R + L/2$, where $L = 2\,\mu m$ is the length of the rod. Concerning the short-ranged repulsive force $\vec{F}_{ev}(h,\theta)$ and torque $\vec{\tau}_{ev}(h,\theta)$, which depend on the configuration of a particle, we adopt a numerical approach, due to the complicated shape of the particle. Specifically, we consider a force per unit area on the particle surface, $\vec{f}_{EV} = -F_0(\hat{n}\cdot\hat{z})\,H(-(\hat{n}\cdot\hat{z}))\,e^{-z/H}$, where H is the Heaviside step function and $H = 0.1R$ is chosen as the length scale of the force. The factors of $(\hat{n}\cdot\hat{z})$ account for the orientation of different patches of particle surface with respect to the wall normal; the step function ensures that the areas of the particle facing away from the wall do not contribute to the repulsive force. This force is numerically integrated

over the meshed surface of the particle to obtain the repulsive force and torque. The prefactor F_0 is chosen in non-dimensional form to be $F_0/\mu U_0 R = 500$.

4. Tail length effect

In the framework of the model, we briefly consider the effect of changing the tail length for a particle in unbounded solution. In Fig. S5, we show the dimensionless contributions of the inert face $\tilde{U}_i$ (black curve with diamonds) and the cap $\tilde{U}_c$ (red curve with squares) to the free space velocity as a function of the dimensionless particle end-to-end distance L/R. These quantities are defined by the equation $U_{fs}/U_0 = b_i \tilde{U}_i + b_c \tilde{U}_c$, exploiting the superposition principle. Thus, for the end-to-end distance $L/R = 6$ considered in the modeling in the main text, $\tilde{U}_i = 0.0943$ and $\tilde{U}_c = -0.0298$.

In Fig. S5, it is apparent that $\tilde{U}_c$ and $\tilde{U}_i$ have different functional dependencies on the end-to-end distance for the distances considered. This difference opens the possibility of obtaining a particle length dependent reversal of motion for a judicious choice of the ratio of dimensionless surface mobilities b_i/b_c. Indeed, an example of such a reversal is shown in Fig. S5 for $b_i/b_c = 0.3$ (blue curve with circles). On the other hand, for the particle lengths considered, we obtain this reversal in a relatively narrow band of parameters: $0.2 < b_i/b_c < 0.36$. The chemi-osmotic mechanism hypothesized in Nicholls *et al*. may be less dependent on fine-tuning of microscopic parameters. Overall, these findings point to the need for continued studies that combine modeling and experiments to unravel the dependence of motion reversal and other phenomena on the various physical mechanisms that contribute to particle motion.

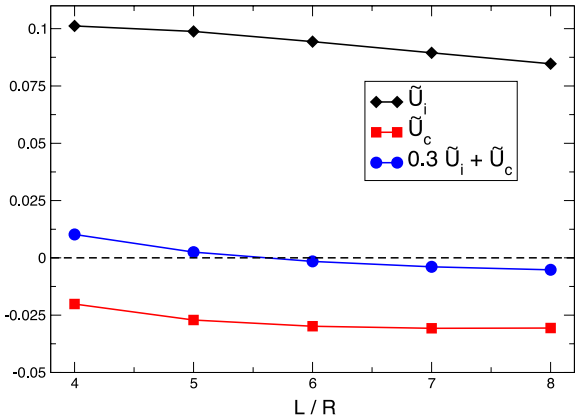

Fig. S5 Tail length dependence of the contribution of the cap (red curve with squares) and the inert face (black curve with diamonds) to the velocity of a particle in unbounded solution. A linear superposition that gives reversal of motion direction is also shown (blue curve with circles).